Materials Today Bio 28 (2024) 101234

Contents lists available at ScienceDirect

Materials Today Bio

journal homepage: www.journals.elsevier.com/materials-today-bio

Analysis of the CPZ/Wnt4 osteogenic pathway for high-bonding-strength composite-coated magnesium scaffolds through transcriptomics

Zewen Shi [a,b,c], Fang Yang [b], Tianyu Du [b], Qian Pang [b], Chen Liu [d], Yiwei Hu [b], Weilai Zhu [b], Xianjun Chen [a], Zeming Chen [a], Baiyang Song [b], Xueqiang Yu [a], Zhewei Ye [c], Lin Shi [a,**], Yabin Zhu [b,***], Qingjiang Pang [a,b,*]

[a] Department of Orthopedics, Ningbo No. 2 Hospital, Ningbo, 315010, PR China
[b] Health Science Center, Ningbo University, Ningbo, 315211, PR China
[c] Department of Orthopaedics, Wuhan Union Hospital, Tongji Medical College, Huazhong University of Science and Technology, Wuhan, 430022, PR China
[d] Ningbo Branch of Chinese Academy of Ordnance Science, Ningbo, 315100, PR China

ARTICLE INFO

Keywords:
Magnesium
Osteogenesis
Polydopamine
High-bonding-strength coating
Carboxypeptidase Z

ABSTRACT

Magnesium (Mg)-based scaffolds are garnering increasing attention as bone repair materials owing to their biodegradability and mechanical resemblance to natural bone. Their effectiveness can be augmented by incorporating surface coatings to meet clinical needs. However, the limited bonding strength and unclear mechanisms of these coatings have impeded the clinical utility of scaffolds. To address these issues, this study introduces a composite coating of high-bonding-strength polydopamine-microarc oxidation (PDA-MHA) on Mg-based scaffolds. The results showed that the PDA-MHA coating achieved a bonding strength of 40.56 ± 1.426 MPa with the Mg scaffold surface, effectively enhancing hydrophilicity and controlling degradation rates. Furthermore, the scaffold facilitated bone regeneration by influencing osteogenic markers such as RUNX-2, OPN, OCN, and VEGF. Transcriptomic analyses further demonstrated that the PDA-MHA/Mg scaffold upregulated carboxypeptidase Z expression and activated the Wnt-4/β-catenin signaling pathway, thereby promoting bone regeneration. Overall, this study demonstrated that PDA can synergistically enhance bone repair with Mg scaffold, broadening the application scenarios of Mg and PDA in the field of biomaterials. Moreover, this study provides a theoretical underpinning for the application and clinical translation of Mg-based scaffolds in bone tissue engineering endeavors.

1. Introduction

In recent years, the incidence of bone defects attributed to physical activities, trauma, and aging has markedly increased [1]. These defects often necessitate the use of bone substitute materials for healing [2]. In clinical practice, titanium alloys are the most frequently used materials for bone substitutes [3]. These alloys exhibit excellent stability, with few complications occurring after implantation in bone defect. This reliability has made titanium alloys a popular choice for bone repair [4]. However, with the increasing number of applications, some drawbacks have surfaced. Titanium alloys are non-degradable, meaning they either stay in the body permanently or need to be removed through second surgery, which can be risky for patients [5]. This leads to a preference for biodegradable materials [6]. Furthermore, their mechanical properties differ from natural bone, causing a stress shielding effect that may lead to bone loss [6]. More importantly, biologically inert titanium alloys lack biological function, preventing them from actively aiding in new bone formation and reconstruction [7]. This limitation reduces their effectiveness in promoting bone repair. Ideally, such bone substitute materials should emulate the mechanical properties of human bone while exhibiting biodegradability, biocompatibility, osteogenesis, and angiogenic capabilities [8].

Magnesium (Mg) has garnered considerable attention owing to its compatibility with the mechanical properties of human bone [9]. In contrast to non-degradable titanium alloys, Mg is a degradable metal, allowing it to avoid a second surgery for removal [5]. Furthermore,

* Corresponding author. Department of Orthopedics, Ningbo No. 2 Hospital, Ningbo, 315010, PR China.
** Corresponding author. Department of Orthopedics, Ningbo No. 2 Hospital, Ningbo, 315010, PR China.
*** Corresponding author. Health Science Center, Ningbo University, Ningbo, 315211, PR China.
E-mail addresses: zhuyabin@nbu.edu.cn (Y. Zhu), pangqingjiang@ucas.ac.cn (Q. Pang).

https://doi.org/10.1016/j.mtbio.2024.101234
Received 16 June 2024; Received in revised form 1 September 2024; Accepted 7 September 2024
Available online 8 September 2024

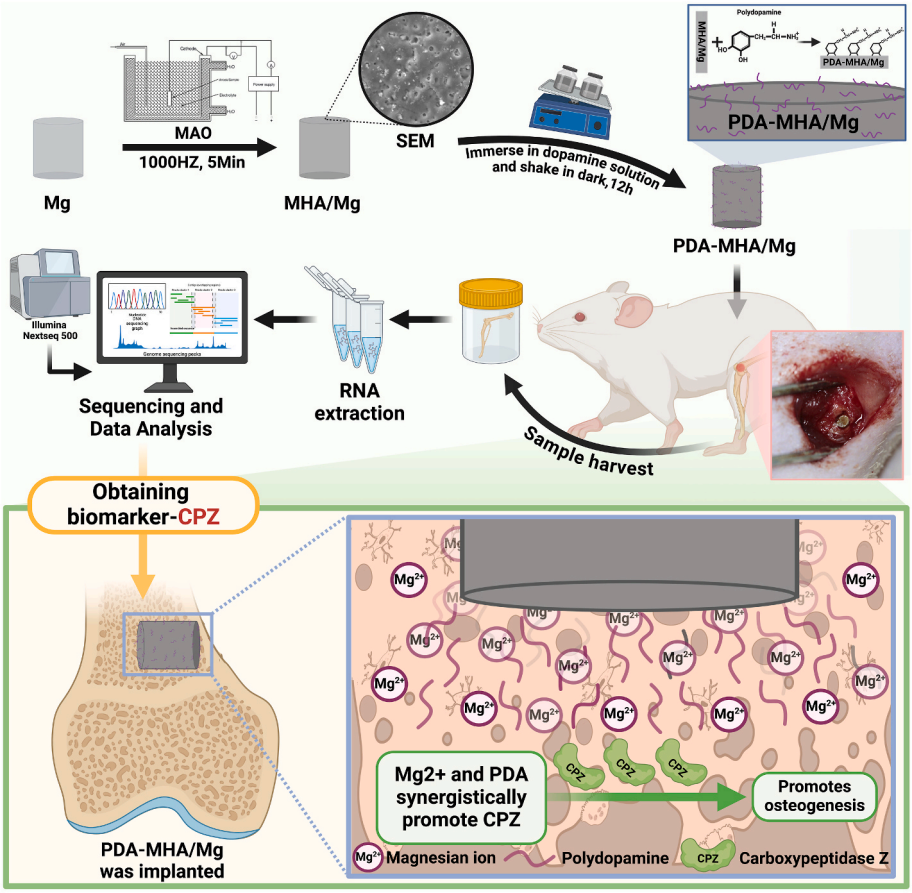

Fig. 1. Schematic illustration of the preparation and property research of PDA-MHA/Mg scaffold.

compared to non-biological titanium alloys, the release of magnesium ions (Mg^{2+}) during its degradation can promote osteogenesis [10] and angiogenesis [11]. Hence, compared to titanium alloy, Mg better aligns with the ideal characteristics of bone substitute materials. However, the rapid degradation rate of Mg can impede tissue regeneration, evidenced by the swift release of hydrogen gas and a rapid increase in pH levels [12]. This degradation also leads to a notable decline in mechanical strength, underscoring the critical need to regulate the degradation rate of Mg scaffolds [13].

Methods for regulating the degradation rate of Mg scaffolds primarily encompass purification, alloying, and surface modification [14]. Among these, surface modification—particularly through coatings—has emerged as the simplest and most effective technique. Various coating preparation methods, such as chemical deposition, electro-deposition, hydrothermal deposition, spraying, electrospinning, and sol-gel techniques have been employed to modulate the degradation rate of Mg scaffolds [15–17]. Despite these advancements, a major challenge persists: the coatings often exhibit insufficient bonding strength to the scaffolds [18,19]. Consequently, long-term detachment occurs, undermining the protective effect of the coatings on the scaffold. Therefore, the development of coatings exhibiting high bonding strength is essential for effectively regulating the long-term degradation rate of Mg scaffolds [20].

In recent developments, micro-arc oxidation coatings (MAO), known for their superior bonding strength, have emerged as a viable approach for regulating the degradation rate of Mg scaffolds [10,21]. However, their porous structure can undermine their protective efficacy [22]. Our previous research demonstrated that incorporating nano-hydroxyapatite (nHA) into the MAO to form an MHA coating can reduce its porosity, thereby enhancing its protective efficacy [23]. To further address this issue, applying a composite coating atop the MAO is often necessary to seal the pores and enhance protection [24]. Additionally, hydroxyapatite, a key inorganic part of bone [6], can stimulate osteoblasts to differentiate and become active, thus hastening the development of new bone tissue in living organisms [25]. As hydroxyapatite has the ability to capture proteins and factors that promote bone growth [6]. Unfortunately, composite coatings frequently exhibit insufficient interfacial bonding strength, leading to detachment and, ultimately, coating failure [26]. Additionally, the preparation procedures for most composite coatings are complex and pose challenges for scalability [27]. The development of a composite coating for Mg scaffolds that is both simple to prepare and exhibits robust bonding strength remains a significant challenge.

In biomedical applications, nature-derived principles are increasingly applied to surface engineering, leading to the development of innovative biomaterials with outstanding biocompatibility, functionality, and performance. Inspired by mussel proteins, polydopamine (PDA) is used to create functional materials and process interfaces [28,29]. In the preparation of the PDA coating, the catechol groups in DA undergo oxidation reactions, producing radicals. These radicals bond covalently or coordinately with the material surface, securing firm adhesion and culminating in the formation of a PDA coating [30]. The PDA coating adheres strongly to substrates, offering effective protection [20]. Moreover, the radical scavenging, antioxidant properties, photoresponsiveness, tissue adhesiveness, physiological stability, biodegradability, excellent biocompatibility, and cellular affinity render PDA uniquely interesting in the field of biomedical sciences.

In this study, we developed a composite coating, denoted as PDA-MHA/Mg, exhibiting high bonding strength when applied to Mg scaffolds. This coating consists of MAO, nHA, and PDA, with the MAO and PDA layer providing robust bonding strength [26]. Our previous study demonstrated that the nHA component fills the pores within the MAO

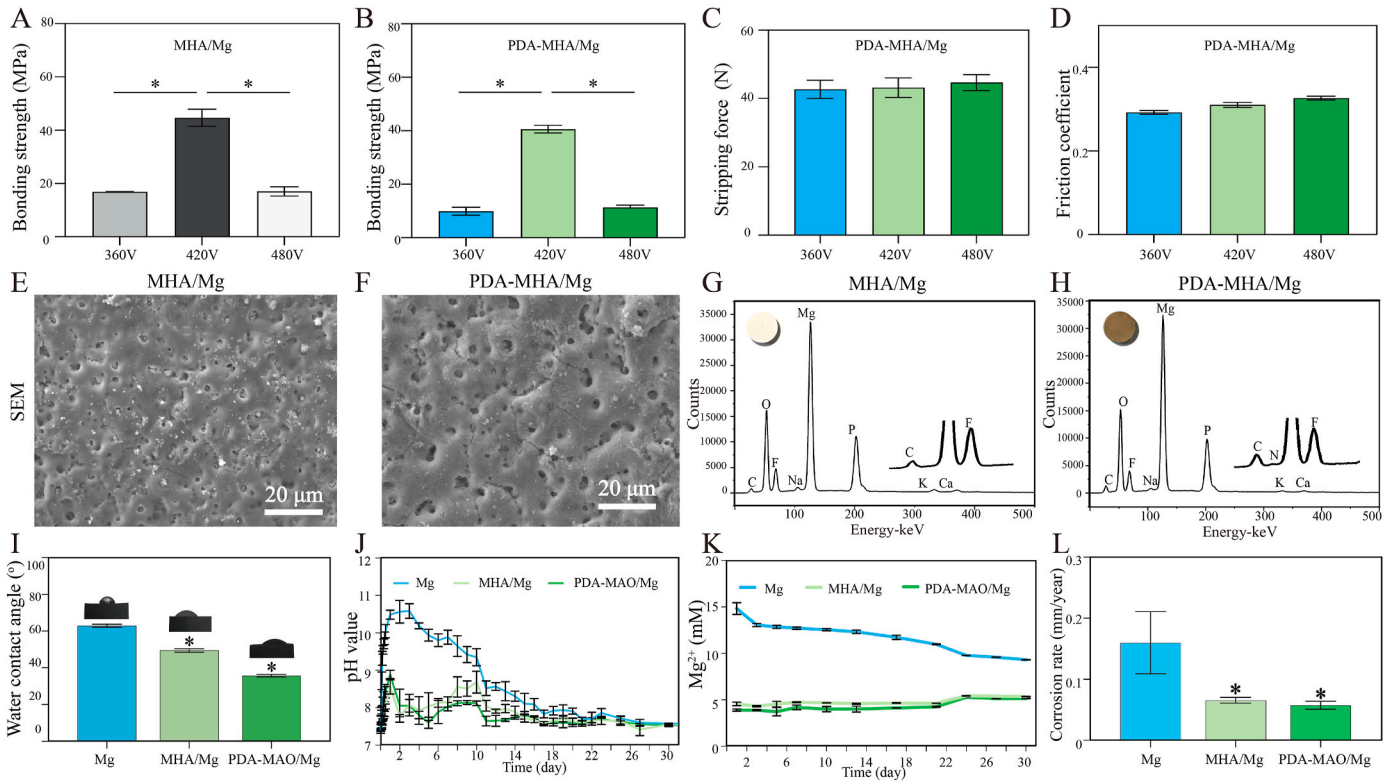

Fig. 2. Characterization and Degradation of PDA-MHA/Mg. (A) Bonding strength of MHA coating. (B) Bonding strength of PDA-MHA coating. (C) Stripping force of PDA-MHA coating. (D) Friction coefficient of PDA-MHA coating. (E) SEM of MHA/Mg. (F) SEM of PDA-MHA/Mg. (G) EDS of MHA/Mg. (H) EDS of PDA-MHA/Mg. (I) Water contact angle. (J) pH value. (K) Mg^{2+} concentration. (L) Corrosion rate. * Indicates statistical significance ($p < 0.05$).

layer, thus furnishing materials essential for bone regeneration [23]. The PDA layer further serves to seal the MAO pores, enhancing endothelial cell adhesion, proliferation, and migration [26]. In this study, both *in vitro* and *in vivo* evaluations demonstrated the ability of the PDA-MHA/Mg scaffold's coating to maintain robust bonding strength while effectively modulating the degradation rate of Mg. Additionally, the scaffold exhibits outstanding biocompatibility and promotes angiogenesis and osteogenesis. Moreover, this study elucidated the mechanisms underlying bone repair facilitated by the PDA-MHA/Mg scaffold employing transcriptomics (Fig. 1). The inter-regulatory relationships among proteins implicated in bone repair were validated through RNA interference (RNAi), quantitative PCR (qPCR), immunofluorescence (IF), and western blot (WB) techniques. Our investigations revealed that the PDA-MHA/Mg scaffold activates carboxypeptidase Z (CPZ) and initiates the Wnt-4/β-catenin signaling pathway, a crucial pathway in bone regeneration. These findings hold significant implications for advancing our understanding of the mechanisms underlying bone repair facilitated by Mg scaffolds.

2. Results and discussion

2.1. Preparation and characteristics of PDA-MHA/mg

An MHA coating was produced using a micro-arc oxidation device on a pure Mg surface. The voltage applied during the production process impacted the bonding strength of the coating [31]. However, the bonding strength of the coating to the substrate is a crucial mechanical property that determines its service life [32]. At 360 V, 420 V, and 480 V, the bonding strength of MHA coatings was 16.89 ± 0.02 MPa, 44.67 ± 3.22 MPa, and 17 ± 1.73 MPa, respectively (Fig. 2A). The bonding strength of the PDA-MHA composite coating was 9.9 ± 1.457 MPa, 40.56 ± 1.426 MPa, and 11.38 ± 0.8083 MPa (Fig. 2B). Firstly, different voltages significantly affect the internal stability of MHA and PDA-MHA coatings, leading to ruptures within the coating and between the coating and substrate. Secondly, at 420V, the bonding strength of MHA and PDA-MHA coatings to the Mg surface was over 40 MPa, significantly higher than the commercial standard of 20 MPa [33]. In addition, comparing to that of the MHA coating, the bonding strength of PDA-MHA composite coating is comparable, due to PDA can create high bonding strength with most surfaces *via* the catechol group [34]. Significantly, at 420V, the bonding strength of both MHA and PDA-MHA coatings exceeded the ISO 13779 standard of 15 MPa by more than threefold [2]. Among the different voltages, the PDA-MHA coating made at 420V exhibits the best internal stability. Besides the bonding strength between the coating and the substrate, scratches on implant surfaces seem unavoidable during surgical procedures. These scratches allow aggressive solutions to infiltrate, causing severe local corrosion and potentially early coating failures [35]. So, the surface stability of the PDA-MHA coating was further evaluated using by scratch and friction test. At 360 V, 420 V, and 480 V, the initial results indicated that the stripping force of the PDA-MHA coating was 42.67 ± 2.66 N, 43.17 ± 2.86 N, and 44.67 ± 2.34 N, respectively, in the scratch test (Fig. 2C). Furthermore, at 360 V, 420 V, and 480 V, the coefficients of friction were 0.292 ± 0.005, 0.313 ± 0.006, and 0.3267 ± 0.005, respectively (Fig. 2D). The scratch and friction test results indicated that the surface stability of the PDA-MHA coating was similar under different voltages (360V, 420V, and 480V) in this study. Thus, different voltages primarily affect the internal stability of the PDA-MHA coating, with minimal impact on surface stability. Considering both internal and surface stability, a voltage of 420V was ultimately chosen to fabricate the PDA-MHA coating.

To confirm the successful application of the PDA-MHA composite coating, we performed both SEM and EDS analyses (Fig. 2E–H). Macroscopically, the PDA-MHA composite coating on the Mg scaffold surface appearedis black, in stark contrast to the white appearance of the MHA coating. This color disparity, attributed to the PDA, suggests

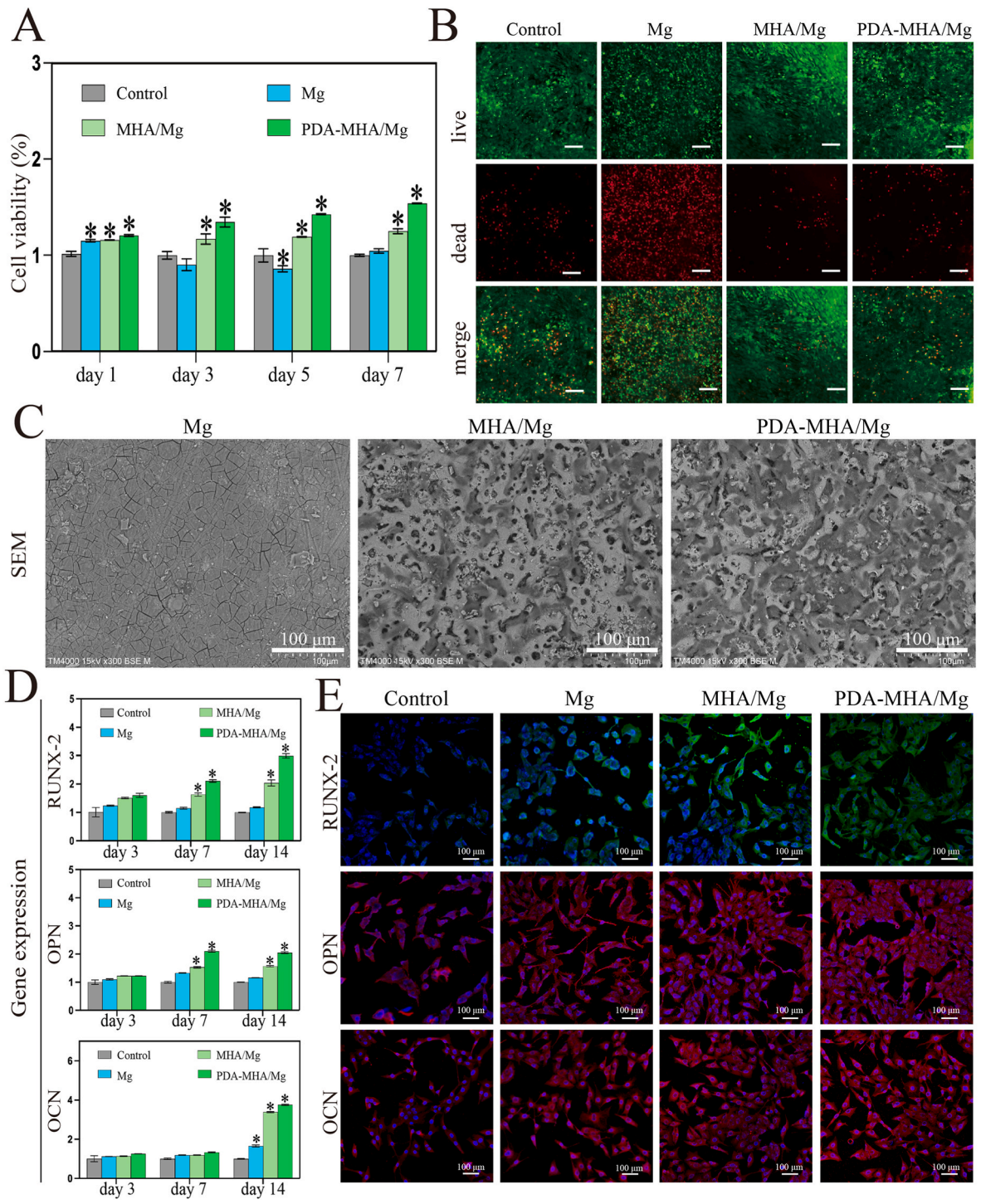

Fig. 3. MC3T3-E1 Compatibility and Differentiation of PDA-MHA/Mg. (A) The viability was tested with CCK-8. (B) The dead cells were tested with Live-Dead Cell Staining Kit. (C) The cell adhesion was tested with SEM. (D) ALP staining. (E) The mineralization was tested by Alizarin red staining. (F) Osteogenesis-related gene expression (RUNX-2, OCN, and OPN) was tested with qPCR on day 3, day 7, and day 14. (G) Immunofluorescent staining with anti-RUNX-2, OPN, and OCN as the primary antibody on day 14. * Indicates statistical significance ($p < 0.05$) compared with the control.

successful adhesion of the PDA on the MHA coating surface. SEM images further corroborated this observation, revealing the successful adhesion of PDA with a discernible reduction in surface particles compared to the MHA coating. Because the particles of MHA are covered by PDA. Additionally, the presence of nitrogen elements detected through EDS analysis of the PDA-MHA coating, which were absent in the MHA coating, confirmed the incorporation of the PDA. These nitrogen elements originated from the PDA, thus validating the successful adhesion of PDA. These observations and analytical results indicated that the PDA-MHA/Mg composite was successfully synthesized.

2.2. *Hydrophilicity and degradation of PDA-MHA/mg*

Enhanced hydrophilicity of biodegradable materials often leads to accelerated degradation rates [36]. Improving surface hydrophilicity without altering the initial rate of degradation presents a challenge. In

this study, water contact angle measurements revealed that Mg exhibited the largest contact angle, followed by the MHA/Mg composite, while the PDA-MHA/Mg exhibited the smallest contact angle (Fig. 2I). These results indicate that PDA-MHA/Mg possesses optimal hydrophilicity, likely attributable to the PDA of the PDA-MHA coating's surface [37]. Due to its many amino groups, polydopamine can create hydrogen bonds with water molecules, giving it strong hydrophilicity. Regarding degradation performance, the pH values, Mg^{2+} concentration, and degradation rates of the MHA/Mg and PDA-MHA/Mg were similar but significantly lower than those of Mg (Fig. 2J–L). This discrepancy arises from Mg's rapid degradation reaction upon direct contact with corrosive ions (such as chloride ions) in PBS solution, whereas a coating can act as an isolating barrier. The hydrophilicity and degradation results indicate that the PDA coating enhanced the hydrophilicity of the MHA/Mg scaffold without accelerating its degradation rate. However, previous studies have shown that increased hydrophilicity leads to accelerated degradation rates [36,38]. This phenomenon is attributed to the sealing of the porous surface of the MHA coating by PDA, which mitigates the increase in degradation rate resulting from improved hydrophilicity. Additionally, in the alkaline environment ensuing from the degradation of PDA-MHA/Mg, PDA can re-adhere to the surface of the scaffold, thus continuing to protect the Mg [39].

2.3. Compatibility of PDA-MHA/mg with human umbilical vein endothelial cells (HUVECs)

While osteocytes primarily control bone formation [40], the vascular endothelial cells also significantly contribute positively to this process [41]. Observations from Supplementary Information Fig. S1A reveal that Mg, MHA/Mg, and PDA-MHA/Mg scaffolds positively affected the viability of HUVECs. Notably, the PDA-MHA/Mg scaffold exhibited the highest level of cell viability. This discrepancy can be attributed to the role of Mg^{2+} in stimulating HUVEC proliferation [42] and the improved biocompatibility of the scaffold owing to PDA [43]. Further assessments, tests including Ttranswell assays and scratch tests (Supplementary Information Figs. S1B and S1C), revealed more pronounced HUVEC migration in the PDA-MHA/Mg group. Moreover, Matrigel tube formation assays (Supplementary Information Fig. S1D) demonstrated that all types of scaffolds facilitated HUVEC tube formation. Notably, the PDA-MHA/Mg scaffold promoted the most robust formation of HUVEC tubes. Mg^{2+} released through the degradation of Mg scaffolds promotes HUVEC growth, migration [44] and tube formation [45], while PDA coatings further enhance the function [46]. PDA in PDA-MHA/Mg helps neutralize free radicals activity, which in turn reduces oxidative stress from excessive free radicals, preventing cell damage [47]. Angiogenesis, as we all understand, depends on the proliferation, migration, and tube formation of vascular endothelial cells [48]. In the process of bone regeneration, angiogenesis is essential because vascularization can also facilitate bone formation [49]. This means that PDA MHA/Mg can stimulate angiogenesis, which in turn accelerates bone formation.

2.4. Compatibility of PDA-MHA/mg with MC3T3-E1 cells

Good biocompatibility is essential for using biomaterials in tissue repair [50]. Therefore, assessing biocompatibility is a crucial criterion in developing any biomaterial for tissue repair purposes [51]. In this study, ensuring the compatibility of biomaterials with osteoblasts is essential for bone repair [41]. This study comprehensively evaluated this compatibility by conducting tests on MC3T3-E1 viability, mortality, and adhesion. Following 24 h of incubation, cell viability was higher in the MHA/Mg and PDA-MHA/Mg groups compared to the control and Mg groups, as shown in Fig. 3A. Moreover, the Mg group exhibited higher cell mortality relative to the other groups (Fig. 3B). This outcome stemmed from the effective regulation of Mg^{2+} release from the Mg scaffold by the MHA and PDA-MHA coatings [52]. Notably, the PDA-MHA/Mg group exhibited the highest increase in cell viability. This is due to the antioxidant properties of the phenolic hydroxyl group in PDA, which can neutralize free radicals, minimize cell damage, and encourage cell growth [51]. The cell adhesion assay revealed that MC3T3-E1 cells exhibited greater adhesion to the surfaces of MHA/Mg and PDA-MHA/Mg compared to the Mg group (Fig. 3C). The rapid degradation of the Mg group resulted in substantial hydrogen gas release, hindering cell adhesion. This occurs because the rapid evolution of hydrogen gas can create microbubbles around the implant, which may physically disrupt the adhesion of cells to the material surface, thereby hindering the initial cellular responses necessary for successful implant integration [53]. Additionally, a greater number of cells adhered to PDA-MHA/Mg compared to MHA/Mg (Fig. 3C), likely attributable to the presence of thin domains of cell adhesion proteins on the biomaterial surface, facilitated by PDA [54]. Overall, the results of viability, mortality, and adhesion tests collectively indicate that PDA-MHA/Mg exhibits the highest compatibility with MC3T3-E1 cells.

2.5. MC3T3-E1 differentiation of PDA-MHA/mg

We investigated the early-stage osteogenic differentiation of MC3T3-E1 cells by quantifying alkaline phosphatase (ALP) expression. As depicted in Fig. 3D, the PDA-MHA/Mg and MHA/Mg group exhibited a significant increase in ALP activity (visible as blue deposits) after 7 days of culture, compared to the Mg and control groups. This is because Mg^{2+} released from the degradation of Mg scaffolds can enhance the ALP activity of osteoblasts [55]. Notably, the Mg group displayed minimal ALP activity, indicating that elevated levels of Mg^{2+} negatively impact the initial stages of osteogenic differentiation [45]. ALP can hydrolyze various types of phosphates and promote cell maturation and calcification. Therefore, we also examined the *in vitro* calcification of osteoblasts [56]. The late-stage osteogenic differentiation of MC3T3-E1 cells was evaluated by measuring ECM mineralization through Alizarin Red S staining following 14 days of culture. The level of ECM mineralization, characterized by red deposits, was elevated in the Mg, MHA/Mg, and PDA-MHA/Mg groups compared to the control, as shown in Fig. 3E. This phenomenon is attributed to the facilitative role of Mg^{2+} in bone mineralization [41]. Additionally, compared to other groups, the PDA-MHA/Mg group showed the highest expression of ALP and bone mineralization. These findings suggest that PDA further augments the promotive effect of Mg^{2+} on MC3T3-E1 cell differentiation [57]. This is because PDA functions akin to the ECM, facilitating increased interactions between cells and biologically functional materials [58], which can affect the function and mineralization of osteoblasts [59].

To further elucidate the mechanisms of differentiation, we investigated the expression of osteogenic differentiation genes and proteins in MC3T3-E1 cells. Genetic analysis revealed a significant increase in the expression of RUNX-2 and OPN in the PDA-MHA/Mg group on day 7 compared to other groups. Additionally, OCN expression was significantly higher in the PDA-MHA/Mg group on day 14, as depicted in Fig. 3F. Furthermore, protein analysis revealed that the PDA-MHA/Mg group displayed the most pronounced expression of osteogenic proteins (RUNX-2, OPN, and OCN), as shown in Fig. 3G. RUNX-2, acting as a transcription factor, plays a pivotal role in osteogenic repair by enhancing the expression of specific osteoblast factors such as OCN and OPN [60]. OPN enhances cellular functions associated with osteogenic differentiation through its interaction with integrin receptors on cell surfaces [61]. While, OCN plays a part in regulating calcium ion deposition and bone mineralization [62]. The results suggest that PDA-MHA/Mg activates RUNX-2, along with the osteogenic markers OPN and OCN, thereby effectively enhancing MC3T3-E1 cell differentiation. This phenomenon is attributed to the influence of Mg^{2+} released from Mg on cellular processes, such as attachment, differentiation, and mineralization, ultimately facilitating osteoblast differentiation [26]. Additionally, PDA regulates cell-cell interactions *via* integrins, thereby enhancing the stability of cell adhesion and the integration of proteins within the ECM, consequently promoting cell differentiation [63].

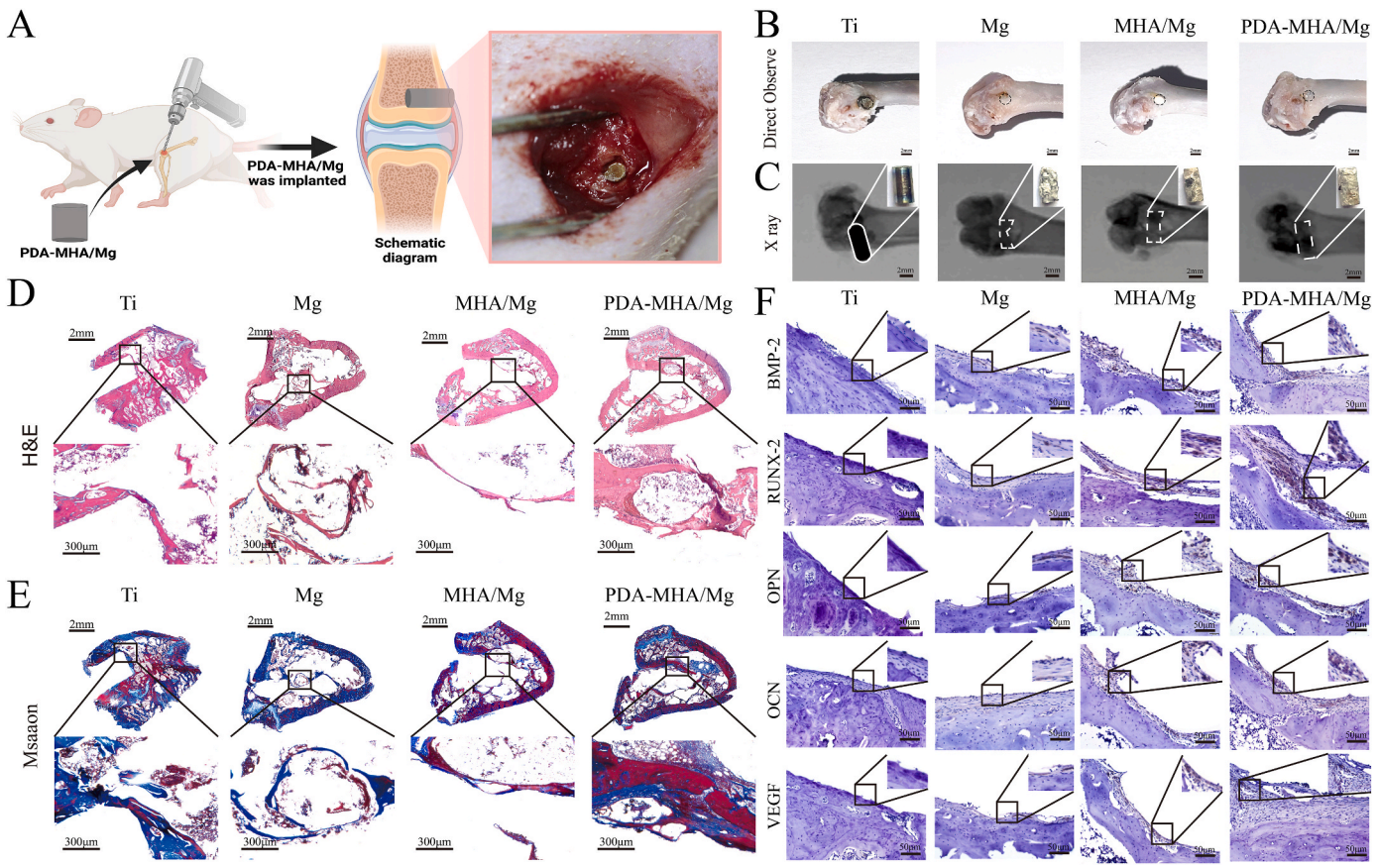

Fig. 4. The Degradation and Osteogenesis of PDA-MHA/Mg *in vivo*. The femoral defect was made and treated by Mg, MHA/Mg and PDA-MHA/Mg, with Ti as the reference. (A) Schematic diagram of animal experiments. (B) Cross view. (C) X-ray and direct observation of scaffold. (D) H&E staining. (E) Masson's trichrome staining. (F) IHC staining.

Furthermore, the functional groups in PDA, promoting protein adsorption [64]. This protein adsorption is vital for initiating and supporting the processes of bone regeneration and integration with host tissue [65].

2.6. *In vivo degradation of PDA-MHA/mg*

As an orthopaedic implant, the rapid degradation of Mg presents a drawback, potentially leading to a rapid decrease in mechanical strength [66]. We investigated the *in vivo* degradation of scaffolds *via* animal experiments. Fig. 4A delineates the detailed procedure and placement of scaffold implantation within the distal femur of rats. Compared to titanium (Ti), the Mg, MHA/Mg, and PDA-MHA/Mg groups exhibited partial degradation of the scaffold along with bone regeneration at the implantation site (Fig. 4B). Similarly, X-ray imaging revealed that the Ti scaffold did not undergo degradation, while the Mg, MHA/Mg, and PDA-MHA/Mg scaffolds exhibited partial degradation (Fig. 4C). Subsequently, the scaffolds were retrieved from the organism, affirming the observations made through X-ray imaging. Additionally, unlike the heterogeneous degradation of Mg and MHA/Mg, the PDA-MHA/Mg exhibited a more homogeneous degradation pattern. This may be due to the alkaline microenvironment produced by Mg degradation, where the phenolic hydroxyl groups in PDA form coordinate bonds with magnesium ions, allowing PDA to reattach to the damaged coating surface [30]. Such homogeneous degradation pattern is desirable to meet the mechanical demands of biodegradable materials employed in bone repair [67]. In essence, the degradation characteristics of the PDA-MHA/Mg render it more apt for fulfilling the requirements of bone repair materials compared to the other groups.

2.7. *In vivo osteogenesis of PDA-MHA/mg*

To investigate the osteogenic potential of PDA-MHA/Mg *in vivo*, we analyzed new bone formation. Fig. 4D and E illustrate the new bone formed around the scaffold. In the Ti group, no new bone formation was observed around the implant. In the Mg group, a minor degree of bone growth was observed, albeit accompanied by bone resorption in the area. The MHA/Mg group exhibited limited new bone formation, with no notable resorption observed. The PDA-MHA/Mg group demonstrated significant new bone formation without any apparent resorption around the scaffold. This suggests that the effects of Mg^{2+} on osteoblasts is concentration-dependent [68]. In addition to previous studies have indicated that Mg^{2+} can promote osteoblast function [69], our study suggests that excessive levels of Mg^{2+} may exert contrary effects. Due to high Mg^{2+} concentrations inhibiting the mineralization of osteoblasts, bone formation is reduced [70].

In this study, we employed IHC to assess the degree of bone formation at the molecular level [71,72]. Fig. 4F illustrates distinct differences in the expression levels of osteogenic markers (BMP-2, RUNX-2, OPN, and OCN) across the groups. Areas exhibiting brown staining were evident around the Mg, MHA/Mg, and PDA-MHA/Mg scaffolds, whereas such staining was absent around the Ti scaffold. Notably, osteogenic protein expression was higher in the PDA-MHA/Mg group compared to the Mg group, indicating a more robust osteogenic response with PDA-MHA/Mg. This disparity can be attributed to the crucial roles of BMP-2, RUNX-2, OPN, and OCN in bone formation. The increased expression of osteogenic protein in PDA-MHA/Mg could be due to the release of Mg^{2+}, improving cell activity and then activating the MAPK and Wnt pathways [9]. In addition, vascular reconstruction plays a crucial role in bone formation *in vivo* [73]. Adequate vascular

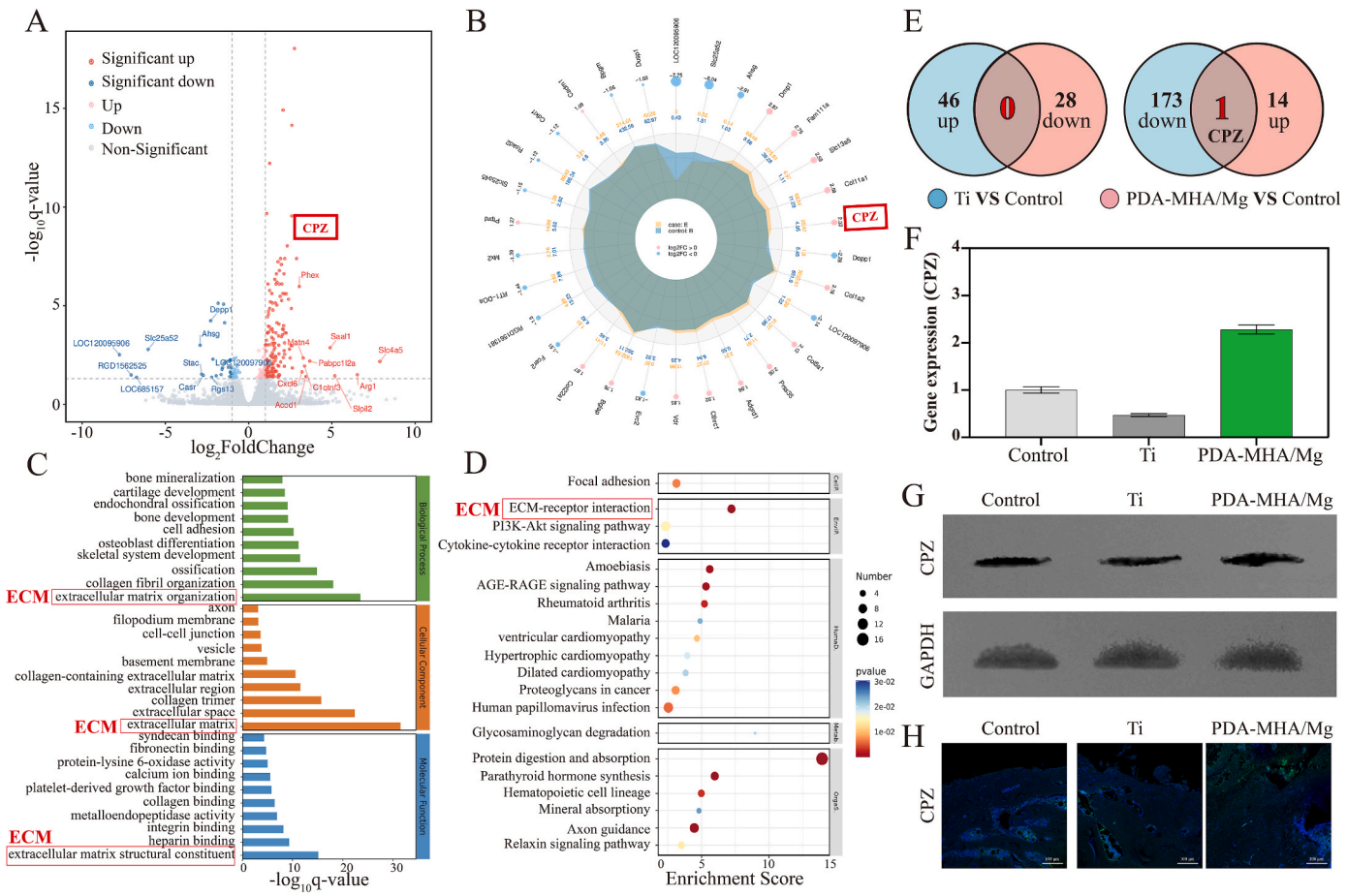

Fig. 5. RNA sequencing of rat femoral bone defect. Comparing DEGs in Ti and PDA-MHA/Mg groups. (A) Volcano map. (B) Radar chart. (C) The GO enrichment analysis of DEGs. (D) The KEGG enrichment analysis of DEGs. Comparing DEGs in control, Ti, and PDA-MHA/Mg groups. (E) Comparing DEGs in control, Ti, and PDA-MHA/Mg groups by Venn diagram. CPZ expression analysis by (F) qPCR. (G) WB. (H) IF.

reconstruction at the implantation site can promote the proliferation and differentiation of osteocytes, thereby favoring new bone formation and remodeling [74]. Our investigation revealed a heightened expression of VEGF in the PDA-MHA/Mg group compared to the other groups (Fig. 4F), suggesting that PDA-MHA/Mg is more effective in stimulating endothelial cell activity for vascular reconstruction. These findings provide reassurance regarding osteogenesis surrounding the PDA-MHA/Mg scaffold.

2.8. *Exploration of osteogenesis mechanisms*

Investigating the mechanisms of biological materials aids in understanding their roles and identifying genes for targeted regulation in precision treatment. Such therapy not only cuts down on economic and time costs but also minimizes patient harm, making it vital to explore mechanisms [40]. Transcriptome analysis is crucial for exploring the mechanisms. Here, we conducted an mRNA transcriptome analysis on femoral bone samples to investigate the mechanism of PDA-MHA/Mg in osteogenesis, employing comparative analysis across different groups. Our investigation revealed 197 differentially expressed genes (DEGs) in the PDA-MHA/Mg group compared to the Ti group. Among these, 165 genes exhibited up-regulation, while 32 genes showed down-regulation ($p < 0.05$, fold change >2). To illustrate these disparities in gene expression, we constructed a differential gene volcano map (Fig. 5A) and radar chart (Fig. 5B), wherein genes were color-coded: red denoting high expression, blue indicating low expression, and grey indicating no significant difference. Notably, we observed a significant difference in the expression of CPZ. CPZ harbors a cysteine-rich domain akin to mammalian Frizzled proteins and functions within the extracellular matrix [75]. This implies a plausible functional analogy between CPZ and Frizzled proteins. Frizzled proteins serve as receptors of the Wnt family, impacting critical cellular processes such as proliferation, differentiation, and migration [75]. Additionally, CPZ's overlapping expression with several Wnt proteins during embryonic stages [75] suggests that CPZ could function as a binding protein akin to Frizzled proteins, interacting with Wnt proteins. To further explore the DEGs, we conducted GO and KEGG enrichment analyses. The GO analysis (Fig. 5C) and KEGG enrichment analysis (Fig. 5D) revealed that the DEGs were predominantly associated with extracellular matrix (ECM). During tissue healing, along with cytokines and growth factors, the ECM influences cell function and plays a crucial role [50]. In bone repair, the ECM also impacts osteoblast function, aiding in bone regeneration [76]. Notably, the ECM is the principal site for CPZ functional activities [77].

To determine whether CPZ is the key gene that plays a major role in the ECM and leads to functional differences between the Ti and PDA-MHA/Mg groups, we conducted further exploration. By analyzing the results of bone healing promotion in various experimental groups *in vivo*, we inferred that CPZ expression in the Ti and PDA-MHA/Mg groups might be reversed compared to the normal group. Therefore, we used Venn analysis to identify whether CPZ is the key gene responsible for the differences between the Ti and PDA-MHA/Mg groups. Employing Venn plot analysis, we found that, in contrast to normal bone tissue, CPZ exhibited a decrease in expression in the Ti group but an increase in the PDA-MHA/Mg group (Fig. 5E). To validate these findings, we examined the expression of CPZ *in vivo* through qPCR and WB. The qPCR and WB analyses demonstrated that CPZ expression was two-fold higher in the

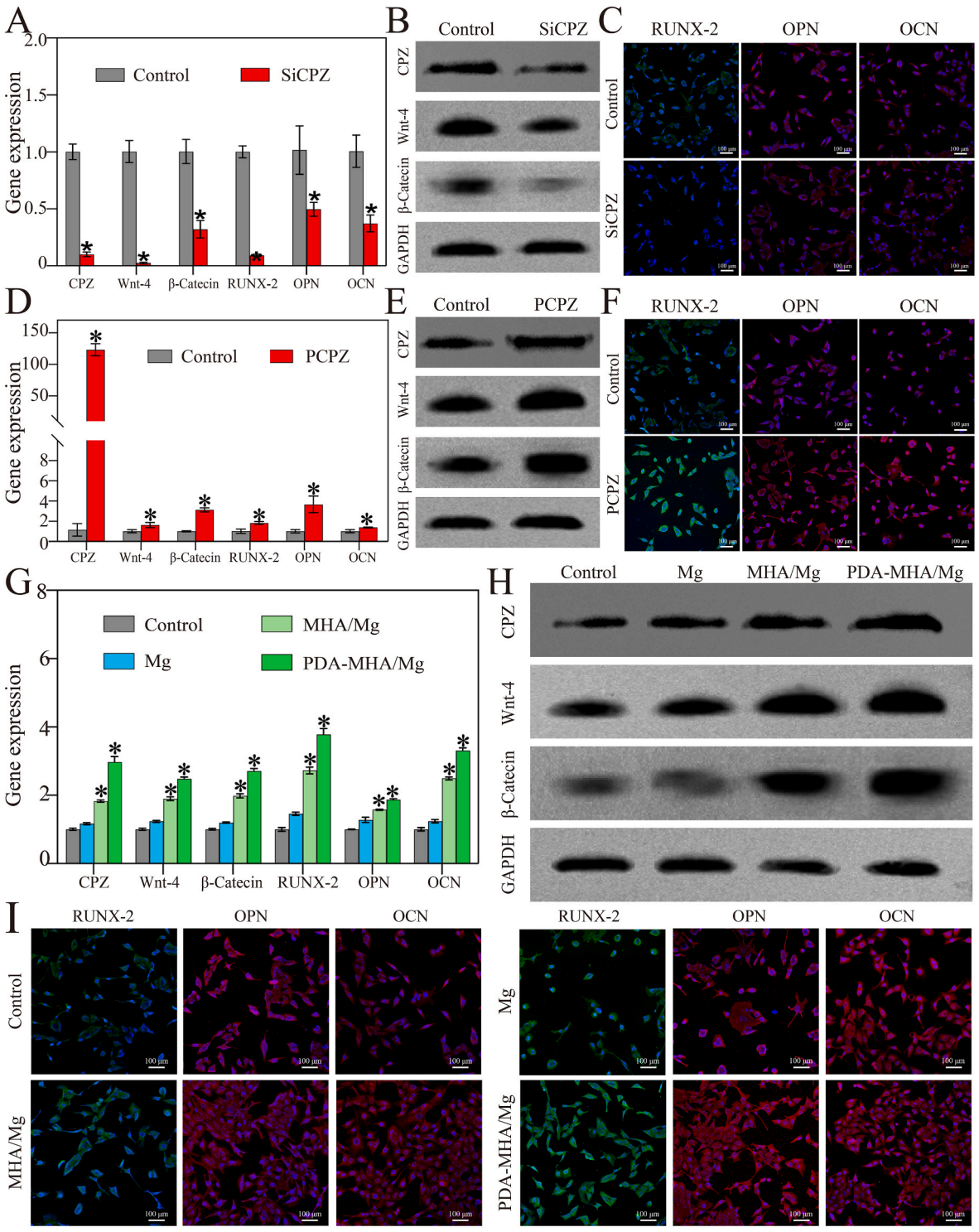

Fig. 6. Osteogenic effects of CPZ on MC3T3E1 cells *via* the Wnt/β-catenin signaling pathway. CPZ silenced by siRNA. Gene expression and protein levels were detected by (A) qPCR. (B) WB. (C) IF. CPZ overexpressed by the plasmid. Gene expression and protein levels were detected by (D) qPCR. (E) WB. (F) IF. CPZ interfered by PDA-MHA/Mg. Gene expression and protein levels were detected by (G) qPCR. (H) WB. (I) IF.

PDA-MHA/Mg group compared to the control group, while in the Ti group, CPZ expression was only half that of the control (Fig. 5F and G). Subsequently, we further examined the location of CPZ expression in tissues using IF. The IF results indicated that CPZ was primarily expressed in the ECM (Fig. 5H), which aligns with our previous hypothesis about key gene. Based on these results, we hypothesized that CPZ may serve as a critical molecule in the osteogenic mechanisms facilitated by PDA-MHA/Mg.

2.9. Validation of osteogenesis mechanisms

The validation of osteogenesis mechanisms comprised two components: assessing the function of CPZ in osteogenesis and investigating the impact of PDA-MHA/Mg on CPZ. To validate CPZ's functionality, we employed siRNA to downregulate its expression in MC3T3-E1 cells. Subsequent qPCR analysis indicated a decrease in the gene expression levels of Wnt-4, β-catenin, RUNX-2, OPN, and OCN following CPZ

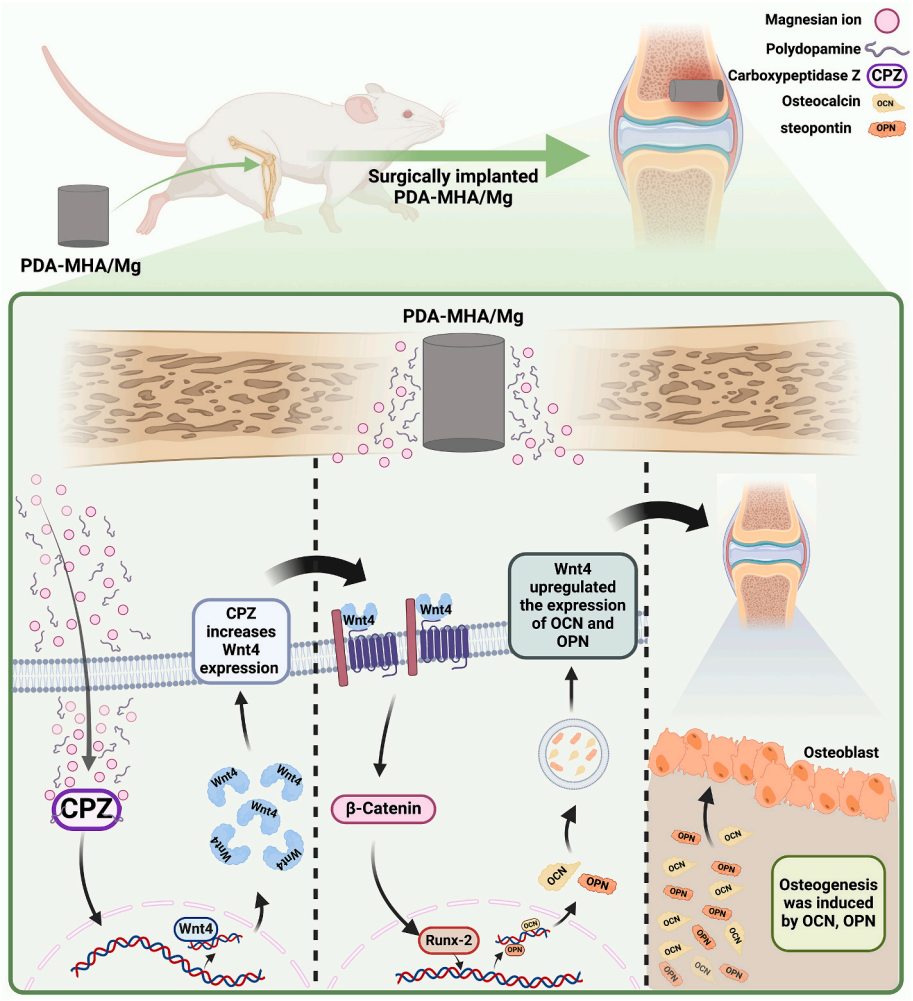

Fig. 7. Schematic diagram of the biological process that enhances bone regeneration through PDA-MHA/Mg.

inhibition (Fig. 6A). WB and IF results aligned with the qPCR outcomes (Fig. 6B and C). To further validate CPZ's functionality, we employed plasmids to enhance its expression in MC3T3-E1 cells. The qPCR analysis demonstrated increased expression of Wnt-4, β-catenin, RUNX-2, OPN, and OCN in MC3T3-E1 cells following CPZ overexpression (Fig. 6D). Consistently, the WB and IF results corroborated the qPCR findings (Fig. 6E and F). Previous studies have demonstrated that CPZ, induced by thyroid hormones, can modulate Wnt/β-catenin signaling and terminal differentiation of growth plate chondrocytes [78]. This study corroborated that CPZ also modulates the Wnt/β-catenin signaling pathway in osteoblasts. However, the Wnt/β-catenin pathway is essential for bone development [79], and its activation of transcription factors such as RUNX-2 can boost bone growth [40]. As demonstrated by this study, the Wnt/β-catenin pathway impacted the expression of osteogenesis-related genes (RUNX-2, OPN, and OCN). Hence, CPZ appears to modulate the osteogenic differentiation of osteoblasts *via* the Wnt/β-catenin pathway.

To assess the impact of PDA-MHA/Mg on CPZ, we employed scaffolds to facilitate direct interactions with MC3T3-E1 cells. The qPCR results showed a significant upregulation in the expression of CPZ, Wnt-4, β-catenin, RUNX-2, OPN, and OCN in the PDA-MHA/Mg group compared to the other groups (Fig. 6G). The WB and IF results were consistent with the qPCR results (Fig. 6H and I). These results indicate that the PDA-MHA/Mg scaffold can activate CPZ, thereby triggering the activation of the Wnt/β-catenin pathway. Earlier studies have demonstrated that Mg^{2+} acts as cofactors for various enzymes, such as those involved in collagen synthesis and matrix metalloproteinases (MMPs) [80], which regulate osteoblast functions by modulating the ECM. This study indicates that, in addition to these enzymes, Mg^{2+} might also serve as crucial cofactors for CPZ, thereby influencing the ECM to promote osteoblast differentiation. Furthermore, studies have shown that PDA has antioxidant properties that generate a low-oxygen environment in adjacent tissues [81]. This environment could potentially enhance the synthesis of thyroid hormones, leading to increased CPZ expression [82]. Our findings suggest that PDA may enhance CPZ expression, thereby promoting osteoblast differentiation.

3. Materials and methods

3.1. Materials

Cylinder Mg (99.99 % purity) was supplied by the Ningbo Branch of the China Academy of Ordnance Sciences (Ningbo, China). Dopamine hydrochloride (DA) was obtained from Macklin Biochemical Technology Co., Ltd. (Shanghai, China), nHA was purchased from Aladdin Biochemical Technology Co., Ltd. (Shanghai, China). The *in vivo* tests were approved by the Management Committee of the Animal Ethics Committee of Ningbo University and were performed at the Ningbo University Animal Experiment Center, utilizing Sprague–Dawley rats (SPF grade) as the test animals. All animal experiments adhered to the guidelines outlined in the National Research Council's Guide for the Care and Use of Laboratory Animals (GB/T 35892-2018). Transcriptome sequencing and subsequent analysis were conducted by OE Biotech Co., Ltd. (Shanghai, China).

3.2. Preparation of PDA-MHA/mg

To obtain MHA/Mg, Cylinder Mg underwent ultrasonic cleaning with ethanol, followed by micro-arc oxidation in an electrolyte solution composed of 3.0 g/L sodium hexametaphosphate, 8.0 g/L potassium fluoride, 10.0 mL/L ethylene glycol, and 1.0 g/L nHA. The applied voltage was varied at 360 V, 420 V, and 480 V, respectively. The oxidizing time was 5 min with a duty cycle of 40.0 % and a frequency of 1000 Hz. Afterwards, we soaked MHA/Mg in a DA/Tris-HCl buffer (pH 8.5) solution with a concentration of 2.0 mg/mL for 12 h, forming PDA-MHA/Mg. We then rinsed the PDA-MHA/Mg with distilled water and left it to dry at room temperature overnight. Detailed methods were described in the Supporting Information.

4. Conclusions

This study introduces a novel PDA-MHA/Mg scaffold with a high-bonding strength composite coating, presenting an effective approach for treating bone defects. Initially, this study demonstrated that the PDA-MHA composite coating improves the surface hydrophilicity of Mg and moderates its degradation rate. Subsequently, this study revealed a significant enhancement in bone regeneration facilitated by the scaffold, as evidenced by the regulation of osteogenic markers, including RUNX-2, OPN, OCN, and VEGF. Transcriptomic analysis further elucidated the molecular mechanisms involved, demonstrating how the PDA-MHA/Mg scaffold upregulates CPZ expression and activates the Wnt-4/β-catenin signalling pathway, which is crucial for bone regeneration (Fig. 7). Overall, the PDA-MHA/Mg scaffold with a simple fabrication process and excellent performance, showing potential for clinical application. Furthermore, the research demonstrated that PDA can synergistically enhance bone repair with Mg, revealing the specific molecular mechanisms involved. This finding significantly broadens the application scenarios of Mg and PDA in the field of biomaterials.

CRediT authorship contribution statement

Zewen Shi: Writing – review & editing, Writing – original draft, Project administration, Methodology, Investigation, Funding acquisition, Formal analysis, Data curation, Conceptualization. **Fang Yang:** Methodology, Investigation, Formal analysis, Data curation. **Tianyu Du:** Methodology, Investigation, Data curation. **Qian Pang:** Methodology, Data curation, Conceptualization. **Chen Liu:** Methodology, Conceptualization. **Yiwei Hu:** Software, Data curation. **Weilai Zhu:** Methodology, Investigation. **Xianjun Chen:** Methodology, Funding acquisition. **Zeming Chen:** Validation, Software, Methodology. **Baiyang Song:** Writing – review & editing, Software. **Xueqiang Yu:** Software, Methodology. **Zhewei Ye:** Project administration, Conceptualization. **Lin Shi:** Writing – review & editing, Project administration, Data curation. **Yabin Zhu:** Writing – review & editing, Visualization, Supervision, Methodology, Formal analysis, Data curation. **Qingjiang Pang:** Writing – review & editing, Supervision, Project administration, Methodology, Funding acquisition, Data curation, Conceptualization.

Declaration of competing interest

The authors declare that they have no known competing financial interests or personal relationships that could have appeared to influence the work reported in this paper.

Data availability

Data will be made available on request.

Acknowledgements and Funding

We acknowledged the financial support from the Postdoctoral Science Foundation of China (2024M751545), National Natural Science Foundation of China (32201139), Major Project of 2025 Sci & Tech Innovation of Ningbo (2020Z096), Natural Science Foundation of Zhejiang (LQ22E020003), Natural Science Foundation of Ningbo (2021J106), Zhejiang Traditional Medicine and Technology Program (2020KY269), Medical Scientific Research Foundation of Zhejiang Province, China (2022KY1129). Key Research Foundation of Hwa Mei Hospital, University of Chinese Academy of Sciences, China (2022HMZD01, 2024HMZD04), Research Foundation of Hwa Mei Hospital, University of Chinese Academy of Sciences (2021HMKY09), Supported by Ningbo Key Specialties of Clinical Features (2024021). Thanks for the technical support by the Core Facilities, Health Science Center of Ningbo University. Thanks to the Laboratory Animal Center of Ningbo University for the technical support. Thanks to the OE Biotech Co., Ltd. for the technical support. Finally, I would like to extend my heartfelt gratitude to my wife, Wenwen Huang, for her unwavering support throughout the years, allowing me to focus on my work.

Appendix A. Supplementary data

Supplementary data to this article can be found online at https://doi.org/10.1016/j.mtbio.2024.101234.

References

[1] B. Fan, et al., Electroactive barium titanate coated titanium scaffold improves osteogenesis and osseointegration with low-intensity pulsed ultrasound for large segmental bone defects, Bioact. Mater. 5 (2020) 1087–1101.
[2] I. Ullah, et al., Mechanical, biological, and antibacterial characteristics of plasma-sprayed (Sr,Zn) substituted hydroxyapatite coating, ACS Biomater. Sci. Eng. 6 (2020) 1355–1366.
[3] R.M. Sabino, G. Mondini, M.J. Kipper, A.F. Martins, K.C. Popat, Tanfloc/heparin polyelectrolyte multilayers improve osteogenic differentiation of adipose-derived stem cells on titania nanotube surfaces, Carbohydr. Polym. 251 (2021) 117079.
[4] S. Wang, et al., Surface modification of titanium implants with Mg-containing coatings to promote osseointegration, Acta Biomater. 169 (2023) 19–44.
[5] N. Zhang, et al., The effect of different coatings on bone response and degradation behavior of porous magnesium-strontium devices in segmental defect regeneration, Bioact. Mater. 6 (2021) 1765–1776.
[6] Y. Bian, et al., Bone tissue engineering for treating osteonecrosis of the femoral head, Exploration 3 (2023) 20210105.
[7] C. Xia, et al., Enhanced physicochemical and biological properties of C/Cu dual ions implanted medical titanium, Bioact. Mater. 5 (2020) 377–386.
[8] M. Rahman, N.K. Dutta, N. Roy Choudhury, Magnesium alloys with tunable interfaces as bone implant materials, Front. Bioeng. Biotechnol. 8 (2020) 564.
[9] J. Xu, et al., Magnesium implantation or supplementation ameliorates bone disorder in CFTR-mutant mice through an ATF4-dependent Wnt/β-catenin signaling, Bioact. Mater. 8 (2022) 95–108.
[10] X. Li, et al., A magnesium-incorporated nanoporous titanium coating for rapid osseointegration, Int J Nanomedicine 15 (2020) 6593–6603.
[11] M. Pei, et al., Sustained release of hydrogen and magnesium ions mediated by a foamed gelatin-methacryloyl hydrogel for the repair of bone defects in diabetes, ACS Biomater. Sci. Eng. 10 (2024) 4411–4424.
[12] M.-H. Kang, et al., Biomimetic porous Mg with tunable mechanical properties and biodegradation rates for bone regeneration, Acta Biomater. 84 (2019) 453–467.
[13] J. Liu, et al., Biodegradable magnesium alloy WE43 porous scaffolds fabricated by laser powder bed fusion for orthopedic applications: process optimization, in vitro and in vivo investigation, Bioact. Mater. 16 (2022) 301–319.
[14] S. Dutta, S. Gupta, M. Roy, Recent developments in magnesium metal-matrix composites for biomedical applications: a review, ACS Biomater. Sci. Eng. 6 (2020) 4748–4773.
[15] B. Yuan, et al., Construction of a magnesium hydroxide/graphene oxide/hydroxyapatite composite coating on Mg-Ca-Zn-Ag alloy to inhibit bacterial infection and promote bone regeneration, Bioact. Mater. 18 (2022) 354–367.
[16] Y. Zhao, et al., pH/NIR-responsive and self-healing coatings with bacteria killing, osteogenesis, and angiogenesis performances on magnesium alloy, Biomaterials 301 (2023) 122237.
[17] Y. Zhang, et al., Defect-free metal-organic framework membrane for precise ion/solvent separation toward highly stable magnesium metal anode, Adv Mater 34 (2022) e2108114.
[18] Y. Lin, et al., Enhanced corrosion resistance and bonding strength of Mg substituted β-tricalcium phosphate/Mg(OH)2 composite coating on magnesium alloys via one-step hydrothermal method, J. Mech. Behav. Biomed. Mater. 90 (2019) 547–555.
[19] J. Tian, X. Qi, C. Li, G. Xian, Mussel-Inspired fabrication of an environment-friendly and self-adhesive superhydrophobic polydopamine coating with excellent mechanical durability, anti-icing and self-cleaning performances, ACS Appl. Mater. Interfaces 15 (2023) 26000–26015.

[20] C. Wu, et al., Clinoenstatite coatings have high bonding strength, bioactive ion release, and osteoimmunomodulatory effects that enhance in vivo osseointegration, Biomaterials 71 (2015) 35–47.
[21] W. Yang, et al., Adhesion, biological corrosion resistance and biotribological properties of carbon films deposited on MAO coated Ti substrates, J. Mech. Behav. Biomed. Mater. 101 (2020) 103448.
[22] C.-Y. Li, et al., In vitro corrosion resistance of a Ta2O5 nanofilm on MAO coated magnesium alloy AZ31 by atomic layer deposition, Bioact. Mater. 5 (2020) 34–43.
[23] Z. Shi, et al., An oxidized dextran-composite self-healing coated magnesium scaffold reduces apoptosis to induce bone regeneration, Carbohydr. Polym. 327 (2024) 121666.
[24] W. Shang, et al., Corrosion resistance of micro-arc oxidation/graphene oxide composite coatings on magnesium alloys, ACS Omega 5 (2020) 7262–7270.
[25] Z. Lin, et al., Hydrogenated silicene nanosheet functionalized scaffold enables immuno-bone remodeling, Exploration 3 (2023) 20220149.
[26] Y. Zhou, et al., Multidynamic osteogenic differentiation by effective polydopamine micro-arc oxide manipulations, IJN 17 (2022) 4773–4790.
[27] Y. Guo, H. Qiu, K. Ruan, Y. Zhang, J. Gu, Hierarchically multifunctional polyimide composite films with strongly enhanced thermal conductivity, Nano-Micro Lett. 14 (2021) 26.
[28] E.D. Eren, et al., A novel chitosan and polydopamine interlinked bioactive coating for metallic biomaterials, J. Mater. Sci. Mater. Med. 33 (2022) 65.
[29] B. Lin, et al., Preparation and characterization of dopamine-induced biomimetic hydroxyapatite coatings on the AZ31 magnesium alloy, Surf. Coating. Technol. 281 (2015) 82–88.
[30] L. Han, et al., Mussel-Inspired tissue-adhesive hydrogel based on the polydopamine-chondroitin sulfate complex for growth-factor-free cartilage regeneration, ACS Appl. Mater. Interfaces 10 (2018) 28015–28026.
[31] Q. Du, et al., The effect of applied voltages on the structure, apatite-inducing ability and antibacterial ability of micro arc oxidation coating formed on titanium surface, Bioact. Mater. 3 (2018) 426–433.
[32] W. Cui, G. Qin, J. Duan, H. Wang, A graded nano-TiN coating on biomedical Ti alloy: low friction coefficient, good bonding and biocompatibility, Mater. Sci. Eng. C 71 (2017) 520–528.
[33] Y.C. Yang, E. Chang, Influence of residual stress on bonding strength and fracture of plasma-sprayed hydroxyapatite coatings on Ti-6Al-4V substrate, Biomaterials 22 (2001) 1827–1836.
[34] J. Gao, et al., Mussel-Inspired, underwater self-healing ionoelastomers based on α-lipoic acid for iontronics, Small 19 (2023) e2207334.
[35] Q. Dong, et al., Insights into self-healing behavior and mechanism of dicalcium phosphate dihydrate coating on biomedical Mg, Bioact. Mater. 6 (2021) 158–168.
[36] R.S. Navarro, et al., Biomimetic tubular scaffold with heparin conjugation for rapid degradation in in situ regeneration of a small diameter neoartery, Biomaterials 274 (2021) 120874.
[37] T.-S. Jang, et al., In-vitro blood and vascular compatibility of sirolimus-eluting organic/inorganic hybrid stent coatings, Colloids Surf. B Biointerfaces 179 (2019) 405–413.
[38] Y. Zhang, et al., Self-stabilized hyaluronate nanogel for intracellular codelivery of doxorubicin and cisplatin to osteosarcoma, Adv. Sci. 5 (2018) 1700821.
[39] Z. Yuan, et al., Biocompatible MoS2/PDA-RGD coating on titanium implant with antibacterial property via intrinsic ROS-independent oxidative stress and NIR irradiation, Biomaterials 217 (2019) 119290.
[40] J. Zhou, et al., Biomaterials and nanomedicine for bone regeneration: progress and future prospects, Exploration 1 (2021) 20210011.
[41] D. Hao, et al., A bioactive material with dual integrin-targeting ligands regulates specific endogenous cell adhesion and promotes vascularized bone regeneration in adult and fetal bone defects, Bioact. Mater. 20 (2022) 179–193.
[42] W. Liu, et al., Magnesium promotes bone formation and angiogenesis by enhancing MC3T3-E1 secretion of PDGF-BB, Biochem. Biophys. Res. Commun. 528 (2020) 664–670.
[43] Asselin, J., Hopper, E. R. & Ringe, E. Improving the stability of plasmonic magnesium nanoparticles in aqueous media. Nanoscale 13, 20649–20656.
[44] H. Qi, et al., Co-culture of BMSCs and HUVECs with simvastatin-loaded gelatin nanosphere/chitosan coating on Mg alloy for osteogenic differentiation and vasculogenesis, Int. J. Biol. Macromol. 193 (2021) 2021–2028.
[45] P. Gao, et al., Biofunctional magnesium coated Ti6Al4V scaffold enhances osteogenesis and angiogenesis in vitro and in vivo for orthopedic application, Bioact. Mater. 5 (2020) 680–693.
[46] C. Su, et al., A facile and scalable hydrogel patterning method for microfluidic 3D cell culture and spheroid-in-gel culture array, Biosensors 11 (2021) 509.
[47] Z. Fu, et al., A cyclic heptapeptide-based hydrogel boosts the healing of chronic skin wounds in diabetic mice and patients, NPG Asia Mater. 14 (2022) 99.
[48] C. J, et al., Dipalmitoylphosphatidic acid inhibits breast cancer growth by suppressing angiogenesis via inhibition of the CUX1/FGF1/HGF signalling pathway, J. Cell Mol. Med. 22 (2018).
[49] Y. Li, et al., 3D printing of tricalcium phosphate/poly lactic-co-glycolic acid scaffolds loaded with carfilzomib for treating critical-sized rabbit radial bone defects, Int J Bioprint 7 (2021) 405.
[50] P. Qin, et al., Zn^{2+} cross-linked alginate carrying hollow silica nanoparticles loaded with RL-QN15 peptides provides promising treatment for chronic skin wounds, ACS Appl. Mater. Interfaces 14 (2022) 29491–29505.
[51] Q. Jia, et al., Hydrogel loaded with peptide-containing nanocomplexes: symphonic cooperation of photothermal antimicrobial nanoparticles and prohealing peptides for the treatment of infected wounds, ACS Appl. Mater. Interfaces 16 (2024) 13422–13438.
[52] F. da S. Lima, R.A. Fock, A review of the action of magnesium on several processes involved in the modulation of hematopoiesis, Int. J. Mol. Sci. 21 (2020) E7084.
[53] J. Rao, et al., Gas station in blood vessels: an endothelium mimicking, self-sustainable nitric oxide fueling stent coating for prevention of thrombosis and restenosis, Biomaterials 302 (2023) 122311.
[54] D. Yin, S. Komasa, S. Yoshimine, T. Sekino, J. Okazaki, Effect of mussel adhesive protein coating on osteogenesis in vitro and osteointegration in vivo to alkali-treated titanium with nanonetwork structures, Int J Nanomedicine 14 (2019) 3831–3843.
[55] K. Zhang, et al., Adaptable hydrogels mediate cofactor-assisted activation of biomarker-responsive drug delivery via positive feedback for enhanced tissue regeneration, Adv. Sci. 5 (2018) 1800875.
[56] J. Zhang, W. Zhang, J. Dai, X. Wang, S.G. Shen, Overexpression of Dlx2 enhances osteogenic differentiation of BMSCs and MC3T3-E1 cells via direct upregulation of Osteocalcin and Alp, Int. J. Oral Sci. 11 (2019) 12.
[57] F. Peng, et al., Zn-contained mussel-inspired film on Mg alloy for inhibiting bacterial infection and promoting bone regeneration, Regen Biomater 8 (2021) rbaa044.
[58] R. Luo, et al., In vitro investigation of enhanced hemocompatibility and endothelial cell proliferation associated with quinone-rich polydopamine coating, ACS Appl. Mater. Interfaces 5 (2013) 1704–1714.
[59] W. Singhatanadgit, I. Olsen, A. Young, ICAM-1-mediated osteoblast-T lymphocyte direct interaction increases mineralization through TGF-β1 suppression, J. Cell. Physiol. 238 (2023) 420–433.
[60] Y. Wang, et al., Stichopus japonicus polysaccharide stimulates osteoblast differentiation through activation of the bone morphogenetic protein pathway in MC3T3-E1 cells, J. Agric. Food Chem. 69 (2021) 2576–2584.
[61] J. Wei, et al., Osteopontin mediates glioblastoma-associated macrophage infiltration and is a potential therapeutic target, J. Clin. Invest. 129 (2019) 137–149.
[62] P.S. Lee, et al., The interplay of collagen/bioactive glass nanoparticle coatings and electrical stimulation regimes distinctly enhanced osteogenic differentiation of human mesenchymal stem cells, Acta Biomater. 149 (2022) 373–386.
[63] Y.B. Lee, et al., Polydopamine-mediated immobilization of multiple bioactive molecules for the development of functional vascular graft materials, Biomaterials 33 (2012) 8343–8352.
[64] J. Li, L.N. Barlow, K.N. Sask, Enhancement of protein immobilization on polydimethylsiloxane using a synergistic combination of polydopamine and micropattern surface modification, J. Biomater. Sci. Polym. Ed. 34 (2023) 2376–2399.
[65] S.V. Harb, et al., Effect of silicon dioxide and magnesium oxide on the printability, degradability, mechanical strength and bioactivity of 3D printed poly (Lactic Acid)-tricalcium phosphate composite scaffolds, Tissue Eng Regen Med 21 (2024) 223–242.
[66] Z. Chen, et al., Osteoimmunomodulatory properties of magnesium scaffolds coated with β-tricalcium phosphate, Biomaterials 35 (2014) 8553–8565.
[67] P. Han, et al., In vitro and in vivo studies on the degradation of high-purity Mg (99.99wt.%) screw with femoral intracondylar fractured rabbit model, Biomaterials 64 (2015) 57–69.
[68] L. Wu, B.J.C. Luthringer, F. Feyerabend, A.F. Schilling, R. Willumeit, Effects of extracellular magnesium on the differentiation and function of human osteoclasts, Acta Biomater. 10 (2014) 2843–2854.
[69] L. Wu, F. Feyerabend, A.F. Schilling, R. Willumeit-Römer, B.J.C. Luthringer, Effects of extracellular magnesium extract on the proliferation and differentiation of human osteoblasts and osteoclasts in coculture, Acta Biomater. 27 (2015) 294–304.
[70] Y.-T. Tsao, Y.-Y. Shih, Y.-A. Liu, Y.-S. Liu, O.K. Lee, Knockdown of SLC41A1 magnesium transporter promotes mineralization and attenuates magnesium inhibition during osteogenesis of mesenchymal stromal cells, Stem Cell Res. Ther. 8 (2017) 39.
[71] Y. Pang, L. Liu, H. Mu, V. Priya Veeraraghavan, Nobiletin promotes osteogenic differentiation of human osteoblastic cell line (MG-63) through activating the BMP-2/RUNX-2 signaling pathway, Saudi J. Biol. Sci. 28 (2021) 4916–4920.
[72] F. Xu, et al., The potential application of concentrated growth factor in pulp regeneration: an in vitro and in vivo study, Stem Cell Res. Ther. 10 (2019) 134.
[73] R. Dimitriou, E. Jones, D. McGonagle, P.V. Giannoudis, Bone regeneration: current concepts and future directions, BMC Med. 9 (2011) 66.
[74] Y. Lai, et al., Osteogenic magnesium incorporated into PLGA/TCP porous scaffold by 3D printing for repairing challenging bone defect, Biomaterials 197 (2019) 207–219.
[75] L. Wang, Y.Y. Shao, R.T. Ballock, Carboxypeptidase Z (CPZ) links thyroid hormone and Wnt signaling pathways in growth plate chondrocytes, J. Bone Miner. Res. 24 (2009) 265–273.
[76] A. Pujia, et al., Bergamot polyphenol fraction exerts effects on bone biology by activating ERK 1/2 and wnt/β-catenin pathway and regulating bone biomarkers in bone cell cultures, Nutrients 10 (2018) 1305.
[77] L.D. McDaniel, et al., Common variants upstream of MLF1 at 3q25 and within CPZ at 4p16 associated with neuroblastoma, PLoS Genet. 13 (2017) e1006787.
[78] N.N. Hauer, et al., Evolutionary conserved networks of human height identify multiple Mendelian causes of short stature, Eur. J. Hum. Genet. 27 (2019) 1061–1071.
[79] Y. Wei, et al., miR-424-5p shuttled by bone marrow stem cells-derived exosomes attenuates osteogenesis via regulating WIF1-mediated Wnt/β-catenin axis, Aging (Albany NY) 13 (2021) 17190–17201.

[80] Y.-L. Chen, et al., Relationships of matrix metalloproteinase 1 and a tissue inhibitor of metalloproteinase to collagen Metabolism in Haliotis discus hannai, J. Agric. Food Chem. 70 (2022) 14886–14897.

[81] M.K. Yazdi, et al., Polydopamine biomaterials for skin regeneration, ACS Biomater. Sci. Eng. 8 (2022) 2196–2219.

[82] Y. Gao, et al., Bioinspired porous microspheres for sustained hypoxic exosomes release and vascularized bone regeneration, Bioact. Mater. 14 (2022) 377–388.